Spontaneous splitting of d -wave surface states: Competition between circulating currents and edge magnetization

(article starts on next page)

Spontaneous splitting of *d*-wave surface states: Competition between circulating currents and edge magnetization

Kevin Marc Seja ◉,* Niclas Wall-Wennerdal ◉,* and Tomas Löfwander ◉

Department of Microtechnology and Nanoscience—MC2, Chalmers University of Technology, SE-41296 Göteborg, Sweden

Mikael Fogelström ◉

Department of Microtechnology and Nanoscience—MC2, Chalmers University of Technology, SE-41296 Göteborg, Sweden
and Nordita, KTH Royal Institute of Technology and Stockholm University, Hannes Alfvéns väg 12, 10691 Stockholm, Sweden

Pair-breaking edges of *d*-wave superconductors feature Andreev bound states at the Fermi energy. Since these states are energetically highly unfavorable they are susceptible to effects that shift them to finite energy. We investigate the free energy of two different mechanisms: spontaneous phase gradients in the superconducting order parameter and surface ferromagnetism caused by Fermi liquid interaction effects. We find that the surface magnetization appears at lower temperatures than the spontaneous current flow of the phase-crystal state. The magnetic state can, however, be energetically favorable at lower temperatures for sufficiently strong Fermi liquid effects. Thus, first-order transitions between the two states as function of system temperature are possible, suggesting a rich low-temperature phase diagram in *d*-wave superconductors.

I. INTRODUCTION

The rich physics of unconventional superconductors has been the subject of intense research for many years. A point of particular interest is the topologically protected surface states that have a large impact on the physics of such materials [1–4]. In the case of *d*-wave superconductors, surfaces not aligned with the main crystallographic *a*- and *b*-axes in the plane host Andreev bound states at the Fermi energy. These states result from scattering between lobes of the order parameter with different sign. They carry a substantial spectral weight due to the large degeneracy with respect to the momentum parallel to the surface. As a result, the bound states are energetically unfavorable and any mechanism that can move them away from the Fermi surface will reduce the ground-state energy of the system [2,5]. The Andreev states are experimentally observed as a zero bias tunneling conductance peak (ZBCP) [6–9] and give rise to a paramagnetic Meissner effect [10]. The ZBCP peak has been observed to split into two separate ones in the presence of external magnetic fields but also spontaneously, i.e., without external field, at low temperatures [11–13]. Over the years, different models for the underlying physics have been discussed, such as a subdominant *s*-wave order parameter at the surface. This leads to a local

breaking of time-reversal symmetry and shifts the Andreev bound states away from the Fermi energy [14,15]. As a competing mechanism, the possibility of ferromagnetic ordering at surfaces was suggested to appear due to electron-electron interaction [5]. At zero temperature arbitrarily small repulsive interactions lead to spin splitting of surface states and a resulting magnetization. This has been shown to be energetically favorable compared to subdominant *s*-wave order [16]. An underlying assumption in the scenarios above is translational invariance along the surface. This disallows another possible mechanism, the spontaneous development of spatially non-trivial phase gradients in the *d*-wave order parameter [17]. This phase-crystal state exhibits a periodic modulation of the phase, characterized by a wave vector **q**, and associated current flow. The surfaces states are then Doppler-shifted away from the Fermi energy and the resulting free energy gain at the surface exceeds the cost of the loop currents in the interior of the sample [18,19]. Strong correlations have been shown to stabilize the phase crystal, even in the presence of disorder [20]. In Refs. [17–20] spin degeneracy was assumed which neglects the possibility of magnetic ordering. It is thus an open question which of the two scenarios is going to be dominant, especially at experimentally relevant finite temperatures.

In the present work we thus allow for both spontaneous phase gradients, as well as magnetic ordering at the surface. To this end, we consider a thin *d*-wave film at finite temperatures and for different magnetic interaction strengths to determine the state with minimal free energy. Our method of choice is the quasiclassical theory of superconductivity. This theory provides an appropriate description of phenomena on the length scale of the superconducting coherence length ξ_0 while neglecting variations on the microscopic length scale of the Fermi wavelength λ_F. Both the surface

---

*These authors contributed equally to this work.

magnetization and the phase-crystal feature typical structure sizes of several coherence lengths and a quasiclassical description is appropriate. A direct comparison between microscopic and quasiclassical descriptions of the phase crystal found universal behavior with minor quantitative differences between the two approaches [19]. Our study shows that the state with minimal energy is usually a phase-crystal state, with magnetic ordering dominating for large magnetic interaction strength and at low temperatures. As function of system temperature, a crossover from one state to the other can occur at a critical temperature that is determined by the strength of Fermi liquid interactions. Our results thus give insight into the competition between the two different orders as well as fingerprints of the different phases.

II. THEORY

A. Quasiclassical theory

For our study, we use the quasiclassical theory of superconductivity in the Eilenberger form [21–23]. We only give a brief overview here, details can be found in our earlier publications [24,25] and other extensive literature [26–28]. In the equilibrium situations considered here, all physical observables of interest can be calculated from the quasiclassical Green's function $\hat{g}^{\mathrm{M}}(\mathbf{p}_{\mathrm{F}}, \mathbf{R}, \varepsilon_n)$ that depends on the momentum direction on the Fermi surface $\mathbf{p}_{\mathrm{F}}$, spatial coordinate $\mathbf{R}$, and the Matsubara frequency ε_n. We obtain $\hat{g}^{\mathrm{M}}$ as a solution to the Eilenberger equation

$$i\hbar\mathbf{v}_{\mathrm{F}} \cdot \nabla \hat{g}^{\mathrm{M}}(\mathbf{p}_{\mathrm{F}}, \mathbf{R}, \varepsilon_n)$$
$$+ [i\varepsilon_n\hat{\tau}_3 - \hat{h}^{\mathrm{M}}(\mathbf{p}_{\mathrm{F}}, \mathbf{R}, \varepsilon_n), \hat{g}^{\mathrm{M}}(\mathbf{p}_{\mathrm{F}}, \mathbf{R}, \varepsilon_n)] = 0, \quad (1)$$

subject to the normalization condition

$$\hat{g}^{\mathrm{M}}(\mathbf{p}_{\mathrm{F}}, \mathbf{R}, \varepsilon_n)\hat{g}^{\mathrm{M}}(\mathbf{p}_{\mathrm{F}}, \mathbf{R}, \varepsilon_n) = -\pi^2. \quad (2)$$

In Eq. (1), a commutator between matrices A and B is denoted $[A, B]$ and ^ indicates a Nambu (particle-hole) space matrix such as the third Pauli matrix $\hat{\tau}_3$. The equation also contains the Fermi velocity $\mathbf{v}_{\mathrm{F}}$ and the self-energy matrix $\hat{h}^{\mathrm{M}}$ that we discuss in detail below. The Green's function $\hat{g}^{\mathrm{M}}$ in Eqs. (1) and (2) is a two-by-two matrix in particle hole space,

$$\hat{g}^{\mathrm{M}} = \begin{pmatrix} g^{\mathrm{M}} & f^{\mathrm{M}} \\ \tilde{f}^{\mathrm{M}} & \tilde{g}^{\mathrm{M}} \end{pmatrix}, \quad (3)$$

with the quasiparticle Green's function on the diagonal and anomalous superconducting correlations on the off-diagonal. Each of the four elements in Eq. (5) is, in turn, a two-by-two matrix in spin space, for example,

$$g^{\mathrm{M}} = \begin{pmatrix} g_0 + g_z & g_x - ig_y \\ g_x + ig_y & g_0 - g_z \end{pmatrix}^{\mathrm{M}} = \begin{pmatrix} g_\uparrow & g_x - ig_y \\ g_x + ig_y & g_\downarrow \end{pmatrix}^{\mathrm{M}}. \quad (4)$$

Objects with a tilde are related to nontilde objects via particle-hole conjugation,

$$\tilde{A}(\varepsilon, \mathbf{p}_{\mathrm{F}}, \mathbf{R}) = A^*(-\varepsilon^*, -\mathbf{p}_{\mathrm{F}}, \mathbf{R}). \quad (5)$$

The self-energy matrix $\hat{h}^{\mathrm{M}}$ has an identical structure in particle-hole and spin space. In this work we consider two self-energy contributions,

$$\hat{h}^{\mathrm{M}} = \hat{h}^{\mathrm{M}}_{\mathrm{MF}} + \hat{h}^{\mathrm{M}}_{\mathrm{FL}}. \quad (6)$$

The first contribution is a spin-singlet, mean-field order parameter

$$\hat{h}^{\mathrm{M}}_{\mathrm{MF}} = \begin{pmatrix} 0 & \Delta_s i\sigma_2 \\ i\sigma_2\tilde{\Delta}_s & 0 \end{pmatrix}. \quad (7)$$

We consider a singlet order parameter Δ_s with d-wave orbital symmetry. Assuming a cylindrical Fermi surface, we parametrize the momentum orientation $\mathbf{p}_{\mathrm{F}}$ via a scalar angle $\phi_{\mathrm{F}} \in [0, 2\pi)$ and can then write

$$\Delta_s(\varphi_{\mathrm{F}}) = \Delta_0\eta_d(\varphi_F) = \Delta_0 \cos(2\varphi_{\mathrm{F}} - 2\alpha), \quad (8)$$

with α being the misalignment angle of the crystallographic a-b axis and the surface normals, while Δ_0 is the (complex) value of the order parameter. The latter is found from the self-consistency equation

$$\Delta_0 = \lambda_d\mathcal{N}_{\mathrm{F}}k_{\mathrm{B}}T \sum_{|\varepsilon_n|<\varepsilon_c} \langle\eta_d(\mathbf{p}_{\mathrm{F}})f^{\mathrm{M}}(\varepsilon_n, \mathbf{p}_{\mathrm{F}})\rangle_{\mathrm{FS}}, \quad (9)$$

where λ_d is the d-wave coupling constant, ε_c is the Matsubara sum cutoff, and we use

$$\langle\ldots\rangle_{\mathrm{FS}} = \int_0^{2\pi} \frac{d\varphi_{\mathrm{F}}}{2\pi}(\ldots), \quad (10)$$

to denote the Fermi-surface average. The second contribution in Eq. (6) is a spin-dependent Fermi-liquid interaction

$$\hat{h}^{\mathrm{M}}_{\mathrm{FL}} = \begin{pmatrix} \boldsymbol{\nu} \cdot \boldsymbol{\sigma} & 0 \\ 0 & \boldsymbol{\nu} \cdot \boldsymbol{\sigma}^* \end{pmatrix}. \quad (11)$$

Following Refs. [26,29,30], the element $i \in \{x, y, z\}$ of $\boldsymbol{\nu}$ is

$$\nu_i \equiv A_{0,i}k_{\mathrm{B}}T \sum_n \langle\mathrm{Tr}_\sigma \ \sigma_i g^{\mathrm{M}}\rangle_{\mathrm{FS}}. \quad (12)$$

Here, Tr_σ is a trace over spin space. While ν_i has the dimension of energy, $A_{0,i}$ is a dimensionless scalar parameter that specifies the strength of the Fermi-liquid interaction along the spin axis i. It is related to the first spin-antisymmetric Landau parameter F_0^a as

$$A_0 = \frac{F_0^a}{1 + F_0^a}, \quad (13)$$

and displays a ferromagnetic Stoner instability for $F_0^a \to -1$ [31]. For simplicity, we assume that a nonzero $A_{0,i}$ exists only along the spin-quantization axis which we label z. Generally, the interaction is ferromagnetic for negative values of A_0, so we replace $A_{0,z} \to -|A_0|$ and specify $|A_0|$ in the following [30]. Assuming an antiferromagnetic interaction (positive $A_{0,z}$) results in a vanishing Fermi-liquid self-energy in our system. In total we thus have a self-energy contribution

$$\nu_z = -2|A_0|k_{\mathrm{B}}T \sum_n \langle g_z\rangle_{\mathrm{FS}}. \quad (14)$$

To solve Eq. (1) we use a Riccati parametrization for the Green's function $\hat{g}^M$ [32–35], and a finite-element method (FEM) that, compared to previous work [25], is here extended to systems with full spin structure. Details on this extended method can be found in the Appendix. To ensure that physical conservation laws are satisfied we solve for both the self-energies as well as the Green's function until self-consistency [24,36]. These self-consistent solutions all show a suppression

of the order parameter near pair-breaking surfaces. At low temperatures a nonzero Fermi liquid self-energy arises in the vicinity of the surfaces. Once a self-consistent solution has been found, we calculate the difference in free energy from the normal state $\Delta\Omega_{\text{LW}} = \Omega_S - \Omega_N$ using the Luttinger-Ward form of the free energy. Following Refs. [26,37–40], we arrive at

$$\Delta\Omega_{\text{LW}} = \Omega_S - \Omega_N$$
$$= \frac{1}{2}k_{\text{B}}T\sum_{\varepsilon_n}\left(\int_0^1\langle\text{Tr}\hat{h}\hat{g}_\lambda\rangle_{\text{FS}}d\lambda - \frac{1}{2}\langle\text{Tr}\hat{h}\hat{g}\rangle_{\text{FS}}\right). \quad (15)$$

Here, $\hat{h}$ and $\hat{g}$ are the self-consistently determined self-energies and Green's function, respectively. In contrast, $\hat{g}_\lambda$ is a solution of Eq. (1) for scaled self-energies, $\hat{\Sigma} \rightarrow \lambda\hat{\Sigma}$, meaning a scaling of all self-energies from zero to the original value. Note that the boundary values of the Green's function have to be iteratively found for this scaled problem, while the self-energies are kept at a fixed scaling of the self-consistent solution. In the present case, we have a spin-singlet order parameter Δ_s and a diagonal self-energy that is proportional to σ_z, thus

$$\text{Tr }\hat{h}\hat{g} = 2(\nu_z g_z + \tilde{\nu}_z\tilde{g}_z - f_s\tilde{\Delta}_s - \tilde{f}_s\Delta_s), \quad (16)$$

with a similar expression for the term $\hat{h}\hat{g}_\lambda$.

Last, we calculate the spin-resolved density of states by solving Eq. (1) for the retarded Green's function. To this end, we replace $i\varepsilon_n \rightarrow \varepsilon + i\eta$, in this work we use $\eta = 0.01k_{\text{B}}T_c$ as a broadening parameter. From the retarded Green's function we obtain the Fermi-surface averaged density of states for spin component $\sigma = \uparrow, \downarrow$ as

$$\mathcal{N}_{\uparrow(\downarrow)}(\mathbf{R}, \varepsilon) \equiv -\frac{\mathcal{N}_{\text{F}}}{2\pi}\langle\text{Im } g^R_{\uparrow(\downarrow)}(\mathbf{p}_{\text{F}}, \mathbf{R}, \varepsilon)\rangle_{\text{FS}}, \quad (17)$$

where ε is the quasiparticle energy, $\mathcal{N}_{\text{F}}$ is the normal-state density of states at the Fermi level and $g_{\uparrow(\downarrow)}$ is defined in Eq. (4). The full density of states is then

$$\mathcal{N}(\mathbf{R}, \varepsilon) = \mathcal{N}_\uparrow(\mathbf{R}, \varepsilon) + \mathcal{N}_\downarrow(\mathbf{R}, \varepsilon). \quad (18)$$

B. Calculational strategy

Our calculations proceed as follows. We initially assume a uniform order parameter and in-plane magnetic field that enters Eq. (1) as a Zeeman-term $\Sigma_{\text{Zeeman}} = \sigma_z h_Z = \mu_B B_{\text{ext}}$. This field serves as a seed for the surface magnetization by creating a spin splitting everywhere in the system. After ten self-consistency iterations, we remove the external field by setting $B_{\text{ext}} = 0$. We now solve Eq. (1) and update the self-energies via Eqs. (9) and (14) until a self-consistent solution is found. Depending on the strength of the Fermi liquid interaction, $|A_0|$, the magnetization at the surface then either disappears, or remains and is present in the final self-consistent solution. For fixed $|A_0|$, we then calculate the free energy using Eq. (15).

C. Model

We consider a thin-film *d*-wave superconductor in two different geometries. First, a strip that is infinite in the *y* direction but has a finite length $L = 40\xi_0$ in the *x* direction, delimited by two fully reflective interfaces. This system is translationally
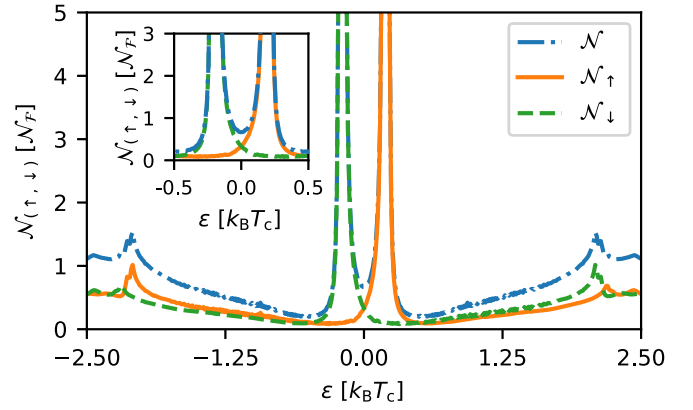

FIG. 1. Fermi liquid interaction effects split the zero-energy Andreev bound states. The full density of states (dash-dotted blue) is split as a result of opposite energy shifts of up-spin (solid orange) and down-spin (dashed green) states. All quantities are shown directly at the surface of a translationally invariant strip with $|A_0| = 0.7$ at $T = 0.15T_c$. Inset: Enlarged view of the main plot around zero energy.

invariant in the *y* direction and quasi-one-dimensional, hence we can solve Eq. (1) along a one-dimensional line. Second, we have a square with sides of length $L = 40\xi_0$ and fully reflective surfaces. In both systems, we assume specular scattering at the surfaces and a misalignment of $\alpha = \pi/4$ between the crystal axes and the respective surface normal [41].

III. RESULTS

A. Translationally invariant strip (1D)

In the translationally invariant system we cannot find a solution with spontaneous current flow. For a strip of width $L = 40\xi_0$ we also do not find signs of the spontaneous symmetry-breaking phases that occur in narrow confined geometries [42]. The only possible transition is then to a magnetized state. At a transition temperature T_M—that depends on $|A_0|$—the surface Andreev bound states are shifted away from the Fermi energy. The spin-resolved density of states for up- and down-spin quasiparticles in Fig. 1 shows that the two peaks are spin polarized, this gives rise to a magnetization at the surface. The energy gained by this bound-state energy shift is larger then the cost of the induced magnetization that extends into the interior of the sample. The surface magnetization can be either of equal or opposite sign at the two edges, both configurations have equal free energy $\Delta\Omega_{\text{LW}}$. The resulting free energy difference is shown in Fig. 2 for several values of $|A_0|$. Both $\Delta\Omega_{\text{LW}}$ and its derivative indicate a second-order phase transition to the magnetically ordered state at T_M. The inset of Fig. 2 shows the dependence of T_M on the Fermi-liquid parameter $|A_0|$. Clearly, for smaller $|A_0|$ the transition temperature T_M is lowered. This connects to the results of Ref. [16] where, at zero temperature, an infinitesimally weak interaction is sufficient to create surface magnetization.
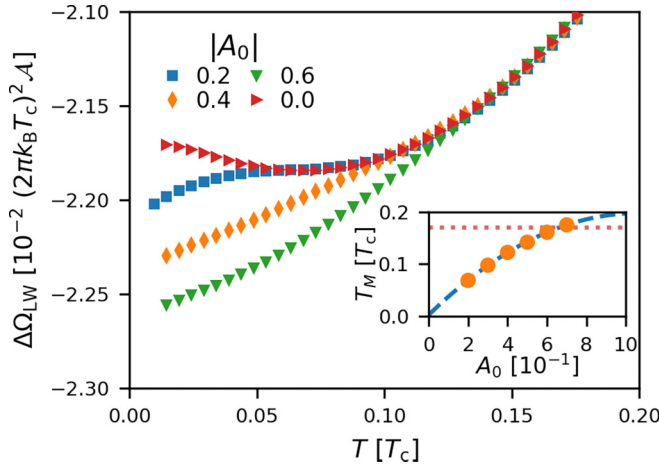
FIG. 2. Free energy $\Delta\Omega_{\mathrm{LW}}$ as function of temperature T in an infinite strip of length $L = 20\xi_0$ in the x direction. In red triangles, the free energy in the absence of magnetic interaction, $|A_0| = 0$, and for finite Fermi-liquid parameter $|A_0|$ as indicated in the legend. Inset: Dependence of T_{M}, the transition temperature to the magnetic state, for various A_0 (orange dots) together with a quadratic fit (blue dashed line) and T^*, the temperature of the phase crystal in the absence of magnetic interaction (red-dotted line).

B. Square geometry (2D)

In a true square geometry we can find two nontrivial and distinct solutions as ground-state candidates. First, a magnetically ordered state with magnetization on all edges, similar to the one found in the infinite strip. Second, we find the so-called phase crystal that features spontaneous phase gradients and currents along the edges. These currents typically flow in pairs of loops that have a radius of around five coherence lengths and carry, per loop-pair, counterflowing current. We find that self-consistent solutions are always either one or the other state and do not observe any mixed states. If the solution is of one or the other type depends on the temperature T and Fermi-liquid interaction strength $|A_0|$.

We start by discussing the magnetic state, shown for one choice of parameters in Fig. 3. As seen in Fig. 3(a), the magnetization is nonuniform along the edges and suppressed close to the grain corners due to interference effects. Figure 3(b) shows that $M_z(\mathbf{R})$ is maximal in the center of each edge and decays exponentially with distance from the surface on the scale of the superconducting coherence length. Similar to the infinite strip, we can find configurations with oppositely pointing magnetic fields at adjacent edges with no difference in free energy. We now turn to the phase crystal state. The main characteristic are spontaneous currents that form loops along the edges, seen in Fig. 4(a). This spontaneous flow is the results of an oscillation of the order-parameter phase shown in Fig. 4(b). For details on the physics of this phase and how such currents can reduce the free energy, we refer to the existing literature [17,18,43]. The underlying solver package for the quasiclassical equations of motion in two dimensions, SUPERCONGA, has been made publicly available [44]. The phase crystal is also found in microscopic models and stabilized when including strong correlations [19,20]. To compare the free energy of the two phases for different temperatures
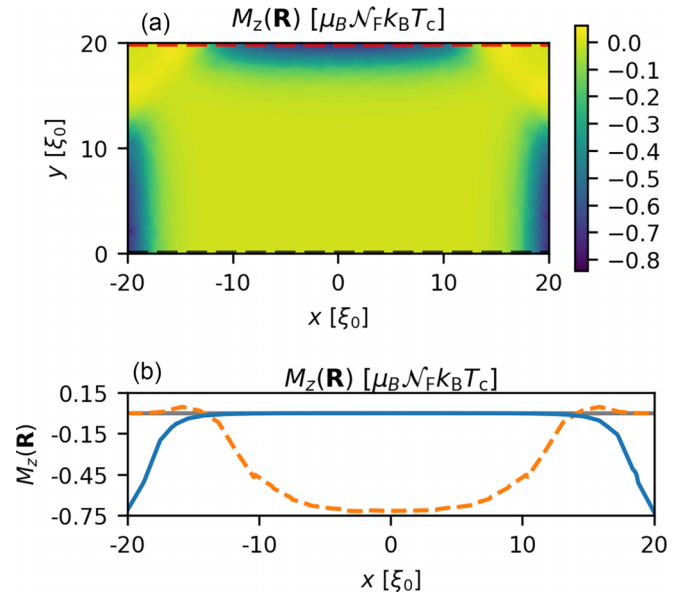

FIG. 3. Surface magnetization for parameters $A_0 = 0.52$ and $T \approx 0.093 T_c$ in a square with an area $\mathcal{A} = (40\xi_0)^2$. In panel (a), a filled contour plot of the magnetization $M_z(\mathbf{R})$, which is symmetric around $y = 0$, in the upper half of the square. In panel (b), in solid blue $M_z(\mathbf{R})$ along $y = 0\xi_0$–seen as a black line in panel (a)—showing the exponential decay into the bulk, and in dashed orange the magnetization along the surface at $y = 20\xi_0$, red line in panel (a), showing the decrease away from the center and small positive value close to the corners.
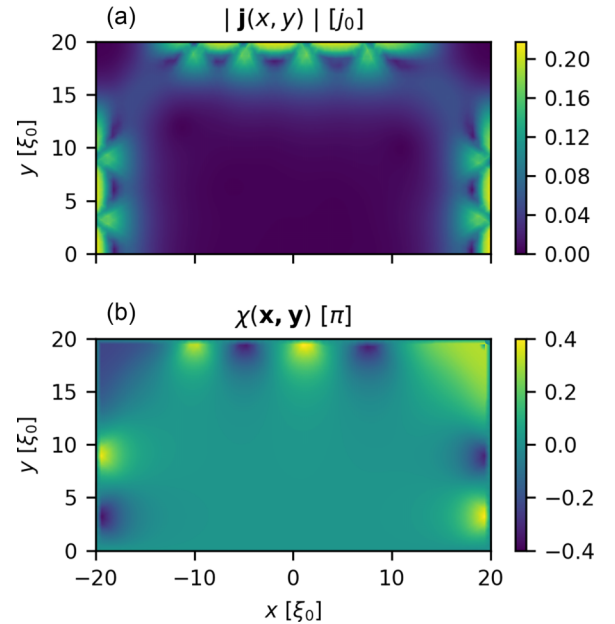

FIG. 4. Example for the phase crystal state in a 2D square with area $\mathcal{A} = L^2 = (40\xi_0)^2$ for $T = 0.1 T_c$. In panel (a), the norm of the current vector $\mathbf{j}(x, y)$ in units of $j_0 = e\mathcal{N}_F \mathbf{v}_F k_B T_c$. In panel (b), the dimensionless phase of the order parameter $\chi(x, y) = \arg(\Delta)$ in units of π. Both quantities are symmetric around $y = 0$ and we show only the upper half of the square.
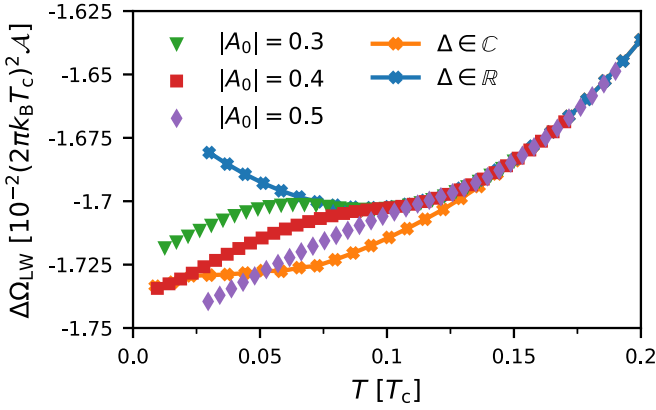
FIG. 5. Free energy $\Delta\Omega_{\mathrm{LW}}$ for finite A_0 as indicated in the legend. Additionally, the case of vanishing A_0 for either a purely real (complex) order parameter marked with blue dots (orange crosses). At sufficiently low temperatures and large enough values of $|A_0|$ the free energy of the magnetic state is lower than that of the phase crystal.

T we consider two sets of parameters. First, we allow for a complex order parameter while Fermi-liquid effects are neglected, $A_0 = 0$, such that only a phase-crystal solution can appear below a critical temperature of $T^* \approx 0.17T_c$ [17]. In a separate set of calculations, we choose a finite $|A_0|$ and force the superconducting order parameter to be real. Depending on temperature, we then find either a magnetized state or a pure d-wave state without current loops. For the sake of comparison, we also calculated the free energy of a system with no magnetic interaction and real order parameter. In this case neither of the two mechanisms shifts the surface bound states and they stay at zero energy. Figure 5 shows the free energy for these different sets of calculations. For finite $|A_0|$, the surface magnetization lowers the free energy below the case of a purely real order parameter (blue line with crosses in Fig. 5). From a purely real order parameter, the state with surface magnetization is reached via a second-order phase transition at a temperature T_M that depends on A_0. This behavior is completely analogous to the infinite strip discussed earlier. In the two-dimensional square geometry, however, we can also find the phase crystal state. For a large temperature range this state with spontaneous current flow has even lower free energy, and is energetically favorable, compared to the state with surface magnetization. For sufficiently large $|A_0|$ and low enough temperature, the magnetic state can have a lower free energy than the phase crystal. In Fig. 5 this is the case for $|A_0| = 0.4$ and $|A_0| = 0.5$. In comparison, for smaller values such as $|A_0| = 0.3$ the phase crystal is always the state with lower free energy. Thus, the prevalence of, e.g., the state with surface magnetization over the phase crystal depends strongly on the strength of Fermi liquid effects in a given material. For conventional superconductors, spin-polarized electron tunneling has been used to experimentally determine $|A_0|$, e.g., for dirty aluminum with a value of $|A_0| = 0.43 \pm 0.1$ [45–47]. An attempt to use similar experimental techniques on YBCO has been reported but gave inconclusive results [48]. What values to expect for typical d-wave materials is thus an open question to experiment. Recent microscopic calculations have

predicted a large increase in the spin susceptibility close to pair-breaking surfaces compared to the bulk in such materials [49]. Since the spin susceptibility is to lowest order given by $\chi_s \propto \mu_F^2 \mathcal{N}^*/(1 + F_0^a)$, this indicates a finite, negative Fermi-liquid parameter F_0^a [31]. The values of Ref. [49] correspond, through Eq. (13), to $A_0 \approx -0.7$ which suggests that a low temperatures a dominance of the magnetic state over the phase crystal is likely. Experimentally, materials with strong enough Fermi liquid interactions should first display a second-order transition to a phase crystal state at $T \approx 0.17T_c$. As temperature is lowered further, a first-order transition to the state with surface magnetization occurs. An experimental fingerprint of the surface-magnetized states is the relatively uniform magnetization along pair-breaking edges compared to the phase crystal that features neighboring circular regions of oppositely pointing magnetic fields generated by the current loop pattern [17]. The two phases should thus be experimentally distinguishable by the magnetic fields generated in the respective case.

IV. DISCUSSION AND OUTLOOK

We have studied the free energy of two distinct ground states in d-wave superconductors. We discussed a state with surface magnetization and another one with orbital currents circulating along the surfaces. In both cases, the free energy of the system is reduced by shifting the surface Andreev bound states to finite energy. At the same time, both the induced currents or magnetization cost energy in the interior of the sample [18]. The balance between the surface and interior free energy contributions determines the transition temperature to either of the two states. Both configurations are reached from a pure d-wave state via second-order phase transitions. For weak Fermi-liquid interaction, the transition to a magnetic state happens at a temperature T_M that is lower than the transition temperature of the phase crystal, $T^* \approx 0.17T_c$. The magnetic state can, however, end up as the ground state for intermediate values of the Fermi liquid parameter and at lower temperatures. Which of the two states ends up being the ground state for given external parameters is determined by material properties, such as the strength of Fermi-liquid effects that renormalize the quasiparticle spectrum. The appearance of a $d \pm ip$-wave state at the surface has been discussed in Ref. [50], an analysis of this is beyond the scope of the present work. Additionally, Fermi liquid interaction beyond the lowest-order s-wave contribution considered here can give rise to spin-orbit coupling and lead to additional splitting or broadening of the surface states. Last, an external magnetic field applied in-plane on a thin film introduces a Zeeman splitting of the density of states. This would make a surface magnetization energetically more favorable while suppressing the phase crystal state. This biasing could thus alter the competition studied in this work and a detailed study would allow for easier comparison to a corresponding experiment.

APPENDIX: DISCONTINUOUS GALERKIN METHOD FOR THE QUASICLASSICAL THEORY WITH GENERAL SPIN STRUCTURE

We give here an overview of a finite-element-based solution strategy to the general Eilenberger equation of quasiclassical theory with the full spin degrees of freedom. This extends a previously reported method for spin-degenerate systems [25]. We focus here on the method for the imaginary-energy, or Matsubara, part of the Green's function that determine the equilibrium properties of a superconducting system. The generalization to nonequilibrium scenarios follows similar lines.

The starting point is a parametrization of the Green's function $\hat{g}^{M}$ in terms of coherence amplitudes γ, $\tilde{\gamma}$ [33,34]. For positive Matsubara frequencies, the Green's function can be written as

$$\hat{g}^{M} = -2\pi i \begin{pmatrix} \mathcal{G} & \mathcal{F} \\ -\tilde{\mathcal{F}} & -\tilde{\mathcal{G}} \end{pmatrix}^{M} + i\pi \hat{\tau}_3 = \begin{pmatrix} g^{M} & f^{M} \\ \tilde{f}^{M} & \tilde{g}^{M} \end{pmatrix}, \quad \text{(A1)}$$

where $\mathcal{G}^{M} \equiv (1 - \gamma^{M}\tilde{\gamma}^{M})^{-1}$ and $\mathcal{F}^{M} \equiv \mathcal{G}^{M}\gamma^{M}$ [28]. In the following, we omit the superscript M to simplify notation. In the previously reported method for spin-degenerate systems, all elements of $\hat{g}$, and hence also the coherence amplitudes, are scalar quantities. For general spin structure, both the Green's function elements and the coherence amplitudes become instead two-by-two matrices in spin space.

We thus obtain a set of four coupled equations that have to be solved. The convention is to write, e.g.,

$$g = \begin{pmatrix} g_0 + g_z & g_x - ig_y \\ g_x + ig_y & g_0 - g_z \end{pmatrix}, \quad \text{(A2)}$$

$$f = \begin{pmatrix} f_0 + f_z & f_x - if_y \\ f_x + if_y & f_0 - f_z \end{pmatrix} i\sigma_2. \quad \text{(A3)}$$

Similarly, we write for the coherence amplitude

$$\gamma = \begin{pmatrix} \gamma_0 + \gamma_z & \gamma_x - i\gamma_y \\ \gamma_x + i\gamma_y & \gamma_0 - \gamma_z \end{pmatrix} i\sigma_2 = \begin{pmatrix} \gamma_1 & \gamma_2 \\ \gamma_3 & \gamma_4 \end{pmatrix} i\sigma_2, \quad \text{(A4)}$$

with an analogous form for $\tilde{\gamma}$. In the following, we will use the latter labeling of the elements of γ in terms of numerical indices $k \in \{1, 2, 3, 4\}$. Similarly, we then label the elements of the self-energy matrices as

$$\Delta = \begin{pmatrix} \Delta_1 & \Delta_2 \\ \Delta_3 & \Delta_4 \end{pmatrix} i\sigma_2, \qquad \Sigma = \begin{pmatrix} \Sigma_1 & \Sigma_2 \\ \Sigma_3 & \Sigma_4 \end{pmatrix}. \quad \text{(A5)}$$

The projections onto singlet (0) or a given triplet (x, y, z) component can be obtained via the reverse linear transformation of Eq. (A4), e.g., for the coherence amplitude

$$\begin{pmatrix} \gamma_0 & \gamma_x \\ \gamma_y & \gamma_z \end{pmatrix} = \frac{1}{2} \begin{pmatrix} \gamma_1 + \gamma_4 & \gamma_2 + \gamma_3 \\ i(\gamma_2 - \gamma_3) & \gamma_1 - \gamma_4 \end{pmatrix}. \quad \text{(A6)}$$

For general complex energies ε, the Riccati equation for the coherence amplitude γ reads

$$i\hbar\mathbf{v}_{\text{F}} \cdot \nabla\gamma = \gamma\tilde{\Delta}\gamma - 2\varepsilon\gamma + \Sigma\gamma - \gamma\tilde{\Sigma} - \Delta, \quad \text{(A7)}$$

with an equation for $\tilde{\gamma}$ that is obtained via Eq. (5). Note that all objects in Eq. (A7) expect for ε are two-by-two spin matrices. Clearly, Eq. (A7) is a nonlinear differential equation for the unknown function γ. We aim to solve it through the iterative solution of a linearized problem using a finite-element method. One possibility to get such an iterative sequence is to assume that the nth iterative guess $\gamma^{(n)}$ is given as a solution to the linearized problem

$$i\hbar\mathbf{v}_{\text{F}} \cdot \nabla\gamma^{(n)} = \gamma^{(n)}\tilde{\Delta}\gamma^{(n-1)} - 2\varepsilon\gamma^{(n)}$$
$$+ \Sigma\gamma^{(n)} - \gamma^{(n)}\tilde{\Sigma} - \Delta. \quad \text{(A8)}$$

Given a starting guess $\gamma^{(0)}$ we then hope that the sequence $\gamma^{(n)}$ will convergence up to a desired accuracy in a reasonable amount of iterations. To unburden the notation, we denote $\Gamma \equiv \gamma^{(n)}$ and $\gamma = \gamma^{(n-1)}$ in the following. Using the labeling of Eqs. (A4) and (A5) and removing factors of $i\sigma_2$, Eq. (A8) leads to an equation system of the form

$$i\hbar\mathbf{v}_{\text{F}} \cdot \nabla\begin{pmatrix} \Gamma_1 & \Gamma_2 \\ \Gamma_3 & \Gamma_4 \end{pmatrix} = \begin{pmatrix} \Gamma_1(-\tilde{\Delta}_4\gamma_1 + \tilde{\Delta}_3\gamma_3) + \Gamma_2(\tilde{\Delta}_2\gamma_1 - \tilde{\Delta}_1\gamma_3) & \Gamma_1(-\tilde{\Delta}_4\gamma_2 + \tilde{\Delta}_3\gamma_4) + \Gamma_2(\tilde{\Delta}_2\gamma_2 - \tilde{\Delta}_1\gamma_4) \\ \Gamma_4(-\tilde{\Delta}_1\gamma_3 + \tilde{\Delta}_2\gamma_1) + \Gamma_3(\tilde{\Delta}_3\gamma_3 - \tilde{\Delta}_4\gamma_1) & \Gamma_4(-\tilde{\Delta}_1\gamma_4 + \tilde{\Delta}_2\gamma_2) + \Gamma_3(\tilde{\Delta}_3\gamma_4 - \tilde{\Delta}_4\gamma_2) \end{pmatrix}$$
$$- 2\varepsilon\begin{pmatrix} \Gamma_1 & \Gamma_2 \\ \Gamma_3 & \Gamma_4 \end{pmatrix} + \begin{pmatrix} \Sigma_1\Gamma_1 + \Sigma_2\Gamma_3 & \Sigma_1\Gamma_2 + \Sigma_2\Gamma_4 \\ \Sigma_3\Gamma_1 + \Sigma_4\Gamma_3 & \Sigma_4\Gamma_4 + \Sigma_3\Gamma_2 \end{pmatrix} - \begin{pmatrix} \Gamma_1\tilde{\Sigma}_4 - \tilde{\Sigma}_2\Gamma_2 & \Gamma_2\tilde{\Sigma}_1 - \Gamma_1\tilde{\Sigma}_3 \\ \Gamma_3\tilde{\Sigma}_4 - \tilde{\Sigma}_2\Gamma_4 & \Gamma_4\tilde{\Sigma}_1 - \Gamma_3\tilde{\Sigma}_3 \end{pmatrix}$$
$$- \begin{pmatrix} \Delta_1 & \Delta_2 \\ \Delta_3 & \Delta_4 \end{pmatrix}. \quad \text{(A9)}$$

Schematically, this system is equivalent to

$$i\hbar\mathbf{v}_{\text{F}} \cdot \nabla\begin{pmatrix} \Gamma_1 \\ \Gamma_2 \\ \Gamma_3 \\ \Gamma_4 \end{pmatrix} = \begin{pmatrix} r_1[\Gamma, \gamma, \Delta, \Sigma] \\ r_2[\Gamma, \gamma, \Delta, \Sigma] \\ r_3[\Gamma, \gamma, \Delta, \Sigma] \\ r_4[\Gamma, \gamma, \Delta, \Sigma] \end{pmatrix} - \begin{pmatrix} \Delta_1 \\ \Delta_2 \\ \Delta_3 \\ \Delta_4 \end{pmatrix}. \quad \text{(A10)}$$

As specified in Eq. (A9) the four right-hand side functions r_k—with $k \in \{1, 2, 3, 4\}$—depend on various elements of Γ, γ, Σ, and Δ, which are in turn spatially dependent. In the following we only write out an explicit spatial dependence of $r_k(\mathbf{R})$. The "driving term," Δ_k, is written out explicitly because it is the only one that is independent of Γ_k. Note also

that the differential operator $\mathbf{v}_F \cdot \nabla$ acts on each element of the four-vector separately. By construction of Eq. (A8) we have a *linear* system of equations for the unknown functions Γ_k in Eqs. (A9) and (A10).

Performing a scalar product of both sides of the equation with a four-vector of, currently unspecified, test functions $\phi = (\phi_1(\mathbf{R}), \phi_2(\mathbf{R}), \phi_3(\mathbf{R}), \phi_4(\mathbf{R}))^T$, and integrating over the domain Ω gives

$$i\hbar \sum_{k=1}^{4} \int_{\Omega} \phi_k(\mathbf{R})[\mathbf{v}_F \cdot \nabla \Gamma_k(\mathbf{R})]\, d\Omega$$

$$= \sum_{k=1}^{4} \int_{\Omega} \phi_k(\mathbf{R})[r_k(\mathbf{R}) - \Delta_k(\mathbf{R})]d\Omega. \quad \text{(A11)}$$

The integration over the domain gets now split up into a sum of integrals over a set of cells T_j that satisfy $\Omega = \cup_{T_j \in \mathcal{T}} T_j$, i.e., over a triangulation $\mathcal{T}$ of the domain Ω. For the transport equation in Eq. (A10) it is crucial to use a so-called *discontinuous Galerkin* method where neighboring cells have independent degrees of freedom associated with each geometric node. This means function values can be different in neighboring cells even at the—geometrically identical—shared cell corners [52,53].

The splitting of the global integral into a sum of per-cell integrals gives

$$i\hbar \sum_{k=1}^{4} \sum_{T_j \in \mathcal{T}} \int_{\Omega_j} \phi_k(\mathbf{R})(\mathbf{v}_F \cdot \nabla \Gamma_k(\mathbf{R}))\, d\Omega_j$$

$$= \sum_{k=1}^{4} \sum_{T_j \in \mathcal{T}} \int_{\Omega_j} \phi_k(\mathbf{R})(r_k(\mathbf{R}) - \Delta_k(\mathbf{R}))d\Omega_j. \quad \text{(A12)}$$

A partial integration of the left-hand side yields

$$i\hbar \sum_{k=1}^{4} \sum_{T_j \in \mathcal{T}} \left[\int_{\partial\Omega_j} \phi_k(\mathbf{R})\Gamma_k(\mathbf{R})\mathbf{v}_F \cdot \mathbf{n}_j\, ds_j \right.$$

$$\left. - \int_{\Omega_j} \Gamma_k(\mathbf{R})\mathbf{v}_F \cdot \nabla \phi_k(\mathbf{R})\, d\Omega_j \right]$$

$$= \sum_{i=1}^{4} \sum_{T_j \in \mathcal{T}} \int_{\Omega_j} \phi_k(\mathbf{R})[r_k(\mathbf{R}) - \Delta_k(\mathbf{R})]d\Omega_j, \quad \text{(A13)}$$

where the first integral is now over the boundary $\partial\Omega_j$ of a cell T_j and contains the edge-dependent, outward-pointing normal vector $\mathbf{n}_j$. A given edge of such a cell will either be on the geometric boundary $\partial\Omega$ or one of the internal edges. We label the collection of such internal edges τ. The geometric boundary $\partial\Omega$ is further split into an inflow boundary $\partial\Omega_-$ and an outflow boundary $\partial\Omega_+$, defined via

$$\partial\Omega_- \equiv \{\mathbf{R} \in \partial\Omega \mid \mathbf{v}_F \cdot \mathbf{n}(\mathbf{R}) < 0\}, \quad \text{(A14)}$$

$$\partial\Omega_+ \equiv \{\mathbf{R} \in \partial\Omega \mid \mathbf{v}_F \cdot \mathbf{n}(\mathbf{R}) \geqslant 0\}. \quad \text{(A15)}$$

The various sets are shown in Fig. 6. The sum over the cell-edge integration then consists of three different types of contributions. First, integrals over edges on the inflow boundary where a boundary value $\Gamma_{k,B}$ has to be specified. We
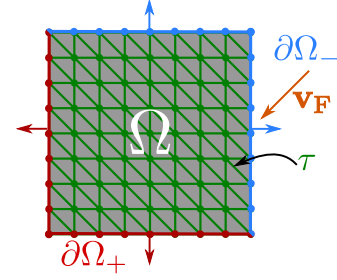

FIG. 6. A domain Ω (gray) with its inflow (outflow) boundary $\partial\Omega_-$ ($\partial\Omega_+$) in marked in light blue (dark red) for the given transport direction $\mathbf{v}_F$ (orange arrow). The collection of internal edges τ is marked in dark green. The mesh nodes of the underlying triangulation is marked by green circles. Small arrows on the domain boundary denote outward-pointing surface normals.

refer to the discussion in Ref. [25] on how these boundary values are found since the procedure is identical to the spin-degenerate case. Second, we have integrals over the outflow boundary where the functions Γ_k are unknown and determined in the later solution procedure. Last, Eq. (A13) features a sum over internal edges. Each edge is integrated over twice, once for each of the two cells that share a given edge. The sign of $\mathbf{n}_j \cdot \mathbf{v}_F$ will be different for the two respective cells which leads to terms proportional to the difference of $\phi_k \Gamma_k$ in the two cells. We will just label two cells sharing an edge as cell 1 and cell 2. It has been shown [54,55] that a numerically stabilized form of rewriting the integral contributions from internal edges in Eq. (A13) is

$$\sum_{k=1}^{4} \sum_{T_j \in \mathcal{T}} \int_{\partial\Omega_j} \phi_k\, (\Gamma_k \mathbf{v}_F) \cdot \mathbf{n}_j\, ds_j$$

$$= \sum_{k=1}^{4} \left(\sum_{\tau_j \in \tau} \int_{\tau_j} \{\Gamma_k(\mathbf{R})\mathbf{v}_F\}_u \cdot [\phi_k(\mathbf{R})]\, d\tau_j \right.$$

$$+ \sum_{s_j \in \partial\Omega_+} \int_{s_j} (\mathbf{n}_j \cdot \mathbf{v}_F)\, \Gamma_k(\mathbf{R})\phi_k(\mathbf{R})\, ds_j$$

$$\left. + \sum_{s_j \in \partial\Omega_-} \int_{s_j} (\mathbf{n}_j \cdot \mathbf{v}_F)\, \Gamma_{k,B}(\mathbf{R})\phi_k(\mathbf{R})\, ds_j \right). \quad \text{(A16)}$$

In Eq. (A16) the first term on the right-hand side originates from the flow through internal edges, the other two terms originate from the domain boundary. The first term contains brackets with a subindex u, $\{\ldots\}_u$, that indicate the so-called upwind value

$$\{\Gamma^R \mathbf{v}_F\}_u \equiv \begin{cases} \Gamma_1^R \mathbf{v}_F & \text{if } \mathbf{v}_F \cdot \mathbf{n}_1 > 0, \\ \Gamma_2^R \mathbf{v}_F & \text{if } \mathbf{v}_F \cdot \mathbf{n}_1 < 0, \\ \{\Gamma^R\}\mathbf{v}_F & \text{if } \mathbf{v}_F \cdot \mathbf{n}_1 = 0. \end{cases} \quad \text{(A17)}$$

This definition and Eq. (A16) contain the jump $[\ldots]$ and average $\{\ldots\}$ of a function along the edge shared by two cells. These bracket operators are defined for vectors $\mathbf{a}$ and scalars

ϕ as

$$[\mathbf{a}] \equiv \mathbf{a}_1 \cdot \mathbf{n}_1 + \mathbf{a}_2 \cdot \mathbf{n}_2, \quad [\phi] \equiv \phi_1 \mathbf{n}_1 + \phi_2 \mathbf{n}_2, \quad (A18)$$

$$\{\mathbf{a}\} \equiv \tfrac{1}{2}(\mathbf{a}_1 + \mathbf{a}_2), \quad \{\phi\} \equiv \tfrac{1}{2}(\phi_1 + \phi_2), \quad (A19)$$

with the function value and the outward-pointing normal vector $\mathbf{n}_j$ in the respective cell labeled by an index (1,2). Effectively, this entire stabilization procedure means that function values are (i) specified on the inflow boundary, (ii) propagated through internal edges along the given transport direction $\mathbf{v}_{\mathrm{F}}$, and (iii) found on the outflow boundary as part of the solution step. This propagation is followed for positive Matsubara poles or the retarded components of the Green's function on the real axis. For advanced components, or negative Matsubara frequencies, the propagation directions swap. In the latter case boundary values are prescribed on the

outflow boundary and values found on the inflow boundary while a downwind value, defined analogously to Eq. (A17), propagates function values through internal edges. In summary, this treatment mirrors the propagation of function values from a starting point to an end point along classical trajectories typically used in finite-difference approaches [28,44,56].

Last, the linear FEM weak form in Eq. (A13) should be written such that all terms containing the unknown functions Γ_k are on the left-hand side while all terms that do not are on the right-hand side of the equation. For our present problem, this means that the inflow-boundary term containing $\Gamma_{k,\mathrm{B}}$ in Eq. (A16) needs to be moved to the right-hand side, while the term containing r_k is moved to the left when combining Eqs. (A13) and (A16). Doing so gives the translation of Eq. (A9) into the corresponding weak form

$$i\hbar \sum_{k=1}^{4} \left[\sum_{\tau_j \in \tau} \int_{\tau_j} \{\Gamma_k(\mathbf{R})\mathbf{v}_{\mathrm{F}}\}_u \cdot [\phi_k(\mathbf{R})] \, d\tau_j + \sum_{s_j \in \partial\Omega_+} \int_{s_j} \mathbf{n}_j \cdot \mathbf{v}_{\mathrm{F}} \, \Gamma_k(\mathbf{R})\phi_k(\mathbf{R}) \, ds_j - \sum_{T_j \in \mathcal{T}} \int_{\Omega_j} \Gamma_k(\mathbf{R})\mathbf{v}_{\mathrm{F}} \cdot \nabla\phi_k(\mathbf{R}) \, d\Omega_j \right]$$

$$- \sum_{k=1}^{4} \sum_{T_j \in \mathcal{T}} \int_{\Omega_j} \phi_k(\mathbf{R}) r_k(\mathbf{R}) d\Omega_j = \sum_{k=1}^{4} \left[-\sum_{T_j \in \mathcal{T}} \int_{\Omega_j} \phi_k(\mathbf{R})\Delta_k(\mathbf{R}) d\Omega_j - \sum_{s_j \in \partial\Omega_-} \int_{s_j} \mathbf{n}_j \cdot \mathbf{v}_{\mathrm{F}} \, \Gamma_{k,B}(\mathbf{R})\phi_k(\mathbf{R}) \, ds_j \right]. \quad (A20)$$

This weak form can now be treated with textbook methods to assemble and solve the corresponding matrix equation system [57]. By solving the resulting system, we obtain a candidate for a new guess Γ for the original nonlinear system in Eq. (A7) under the assumption of previous guess $\gamma = \gamma^{(n-1)}$. In some cases, directly taking the solution Γ as the next iterative guess $\gamma^{(n)}$ is numerically unstable. We observe such instability in particular when solving the transport equations for real energies rather than purely imaginary Matsubara or Ozaki poles [58]. Given a solution Γ_k of the linearized problem, one way to stabilize the iterative procedure is to update $\gamma_k^{(n)}$

via

$$\gamma_k^{(n)} = \gamma_k^{(n-1)} + \alpha\big(\Gamma_k - \gamma_k^{(n-1)}\big). \quad (A21)$$

Here, $\alpha \in (0, 1]$ is a numerical parameter. We find that for general complex energies small values of $\gamma \lesssim 0.4$ are required which increases the number of iterative guesses. Adaptive methods that scale α, e.g., based on the difference between Γ and γ, can lead to faster convergence. In contrast, for purely imaginary poles it is stable to choose $\alpha = 1$, i.e., directly assigning Γ_k as the next guess for $\gamma_k^{(n)}$.

[1] C.-R. Hu, Midgap surface states as a novel signature for d_{xa}^2-x_b^2-wave superconductivity, Phys. Rev. Lett. **72**, 1526 (1994).

[2] T Löfwander, V. S. Shumeiko, and G. Wendin, Andreev bound states in high-T_c superconducting junctions, Supercond. Sci. Technol. **14**, R53 (2001).

[3] S. Ryu and Y. Hatsugai, Topological origin of zero-energy edge states in particle-hole symmetric systems, Phys. Rev. Lett. **89**, 077002 (2002).

[4] M. Sato, Y. Tanaka, K. Yada, and T. Yokoyama, Topology of Andreev bound states with flat dispersion, Phys. Rev. B **83**, 224511 (2011).

[5] C. Honerkamp and M. Sigrist, Time-reversal symmetry breaking states at [110] surfaces of $d_{x^2-y^2}$ superconductors, Physica C: Superconductivity **317-318**, 489 (1999).

[6] T. Becherer, C. Stölzel, G. Adrian, and H. Adrian, Normal electron tunneling in ramp-type YBa$_2$Cu$_3$O$_7$/PrBa$_2$Cu$_3$O$_7$/YBa$_2$Cu$_3$O$_7$ junctions prepared by laser ablation, Phys. Rev. B **47**, 14650(R) (1993).

[7] S. Kashiwaya, Y. Tanaka, M. Koyanagi, H. Takashima, and K. Kajimura, Evidence for d-wave symmetry in high-T_c su-

perconductors based on tunneling theory and STM experiment, Physica C: Superconductivity **235-240**, 1911 (1994).

[8] S. Kashiwaya, Y. Tanaka, M. Koyanagi, H. Takashima, and K. Kajimura, Origin of zero-bias conductance peaks in high-T_c superconductors, Phys. Rev. B **51**, 1350 (1995).

[9] S. Kashiwaya and Y. Tanaka, Tunnelling effects on surface bound states in unconventional superconductors, Rep. Prog. Phys. **63**, 1641 (2000).

[10] S. Higashitani, Mechanism of paramagnetic Meissner effect in high-temperature superconductors, J. Phys. Soc. Jpn. **66**, 2556 (1997).

[11] J. Geerk, X. X. Xi, and G. Linker, Electron tunneling into thin films of Y$_1$Ba$_2$Cu$_3$O$_7$, Z. Phys. B: Condens. Matter **73**, 329 (1988).

[12] J. Lesueur, L. H. Greene, W. L. Feldmann, and A. Inam, Zero bias anomalies in YBa$_2$Cu$_3$O$_7$ tunnel junctions, Physica C: Superconductivity **191**, 325 (1992).

[13] M. Covington, M. Aprili, E. Paraoanu, L. H. Greene, F. Xu, J. Zhu, and C. A. Mirkin, Observation of surface-induced broken

time-reversal symmetry in YBa$_2$Cu$_3$O$_7$ tunnel junctions, Phys. Rev. Lett. **79**, 277 (1997).

[14] M. Matsumoto and H. Shiba, Coexistence of different symmetry order parameters near a surface in *d*-wave superconductors II, J. Phys. Soc. Jpn. **64**, 4867 (1995).

[15] M. Fogelström, D. Rainer, and J. A. Sauls, Tunneling into current-carrying surface states of high-T_c superconductors, Phys. Rev. Lett. **79**, 281 (1997).

[16] A. C. Potter and P. A. Lee, Edge ferromagnetism from Majorana flat bands: Application to split tunneling-conductance peaks in high-T_c cuprate superconductors, Phys. Rev. Lett. **112**, 117002 (2014).

[17] M. Håkansson, T. Löfwander, and M. Fogelström, Spontaneously broken time-reversal symmetry in high-temperature superconductors, Nat. Phys. **11**, 755 (2015).

[18] P. Holmvall, M. Fogelström, T. Löfwander, and A. B. Vorontsov, Phase crystals, Phys. Rev. Res. **2**, 013104 (2020).

[19] N. W. Wennerdal, A. Ask, P. Holmvall, T. Löfwander, and M. Fogelström, Breaking time-reversal and translational symmetry at edges of *d*-wave superconductors: Microscopic theory and comparison with quasiclassical theory, Phys. Rev. Res. **2**, 043198 (2020).

[20] D. Chakraborty, T. Löfwander, M. Fogelström, and A. M. Black-Schaffer, Disorder-robust phase crystal in high-temperature superconductors stabilized by strong correlations, npj Quantum Mater. **7**, 44 (2022).

[21] G. Eilenberger, Transformation of Gorkov's equation for type II superconductors into transport-like equations, Z. Phys. **214**, 195 (1968).

[22] A. Larkin and Y. N. Ovchinnikov, Quasiclassical method in the theory of superconductivity, Sov. Phys. JETP **28**, 1200 (1969).

[23] G. Eliashberg, Inelastic electron collisions and nonequilibrium stationary states in superconductors, Sov. Phys. JETP **34**, 668 (1972).

[24] K. M. Seja and T. Löfwander, Quasiclassical theory of charge transport across mesoscopic normal-metal–superconducting heterostructures with current conservation, Phys. Rev. B **104**, 104502 (2021).

[25] K. M. Seja and T. Löfwander, Finite element method for the quasiclassical theory of superconductivity, Phys. Rev. B **106**, 144511 (2022).

[26] J. W. Serene and D. Rainer, The quasiclassical approach to superfluid ^{3}He, Phys. Rep. **101**, 221 (1983).

[27] N. Kopnin, *Theory of Nonequilibrium Superconductivity* (Oxford University Press, Oxford, UK, 2001).

[28] M. Eschrig, Scattering problem in nonequilibrium quasiclassical theory of metals and superconductors: General boundary conditions and applications, Phys. Rev. B **80**, 134511 (2009).

[29] M. Eschrig, J. A. Sauls, H. Burkhardt, and D. Rainer, Fermi liquid superconductivity, in *High-T_c Superconductors and Related Materials: Material Science, Fundamental Properties, and Some Future Electronic Applications*, edited by S.-L. Drechsler and T. Mishonov (Springer, Dordrecht, The Netherlands, 2001), pp. 413–446.

[30] X. Montiel and M. Eschrig, Generation of pure superconducting spin current in magnetic heterostructures via nonlocally induced magnetism due to Landau Fermi liquid effects, Phys. Rev. B **98**, 104513 (2018).

[31] P. Coleman, *Introduction to Many-Body Physics* (Cambridge University Press, Cambridge, UK, 2015).

[32] Y. Nagato, K. Nagai, and J. Hara, Theory of the Andreev reflection and the density of states in proximity contact normal-superconducting infinite double-layer, J. Low Temp. Phys. **93**, 33 (1993).

[33] N. Schopohl and K. Maki, Quasiparticle spectrum around a vortex line in a *d*-wave superconductor, Phys. Rev. B **52**, 490 (1995).

[34] N. Schopohl, Transformation of the Eilenberger equations of superconductivity to a scalar Riccati equation, arXiv:cond-mat/9804064.

[35] A. Shelankov and M. Ozana, Quasiclassical theory of superconductivity: A multiple-interface geometry, Phys. Rev. B **61**, 7077 (2000).

[36] J. Sánchez-Cañizares and F. Sols, Self-consistent theory of transport in quasi–one-dimensional superconducting wires, J. Low Temp. Phys. **122**, 11 (2001).

[37] J. M. Luttinger and J. C. Ward, Ground-state energy of a many-fermion system. II, Phys. Rev. **118**, 1417 (1960).

[38] E. V. Thuneberg, J. Kurkijärvi, and D. Rainer, Elementary-flux-pinning potential in type-II superconductors, Phys. Rev. B **29**, 3913 (1984).

[39] A. B. Vorontsov and J. A. Sauls, Thermodynamic properties of thin films of superfluid ^{3}He $-A$, Phys. Rev. B **68**, 064508 (2003).

[40] S. Ali, L. Zhang, and J. A. Sauls, Thermodynamic potential for superfluid ^{3}He in aerogel, J. Low Temp. Phys. **162**, 233 (2011).

[41] E. Zhao, T. Löfwander, and J. A. Sauls, Nonequilibrium superconductivity near spin-active interfaces, Phys. Rev. B **70**, 134510 (2004).

[42] A. B. Vorontsov, Broken translational and time-reversal symmetry in unconventional superconducting films, Phys. Rev. Lett. **102**, 177001 (2009).

[43] P. Holmvall, A. B. Vorontsov, M. Fogelström, and T. Löfwander, Broken translational symmetry at edges of high-temperature superconductors, Nat. Commun. **9**, 2190 (2018).

[44] P. Holmvall, N. Wall Wennerdal, M. Håkansson, P. Stadler, O. Shevtsov, T. Löfwander, and M. Fogelström, SuperConga: An open-source framework for mesoscopic superconductivity, Appl. Phys. Rev. **10**, 011317 (2023).

[45] P. M. Tedrow, J. T. Kucera, D. Rainer, and T. P. Orlando, Spin-polarized tunneling measurement of the antisymmetric Fermi-liquid parameter G^0 and renormalization of the Pauli limiting field in A1, Phys. Rev. Lett. **52**, 1637 (1984).

[46] J. A. X. Alexander, T. P. Orlando, D. Rainer, and P. M. Tedrow, Theory of Fermi-liquid effects in high-field tunneling, Phys. Rev. B **31**, 5811 (1985).

[47] R. Meservey and P. M. Tedrow, Spin-polarized electron tunneling, Phys. Rep. **238**, 173 (1994).

[48] H. Kashiwaya, S. Kashiwaya, B. Prijamboedi, A. Sawa, I. Kurosawa, Y. Tanaka, and I. Iguchi, Anomalous magnetic-field tunneling of YBa$_2$Cu$_3$O$_{7-\delta}$ junctions: Possible detection of non-Fermi-liquid states, Phys. Rev. B **70**, 094501 (2004).

[49] S. Matsubara and H. Kontani, Emergence of strongly correlated electronic states driven by the Andreev bound state in *d*-wave superconductors, Phys. Rev. B **101**, 075114 (2020).

[50] S. Matsubara and H. Kontani, Emergence of $d \pm ip$-wave superconducting state at the edge of *d*-wave superconductors mediated by ferromagnetic fluctuations driven by Andreev bound states, Phys. Rev. B **101**, 235103 (2020).

[51] D. Arndt, W. Bangerth, M. Bergbauer, M. Feder, M. Fehling, J. Heinz, T. Heister, L. Heltai, M. Kronbichler, M. Maier, P. Munch, J.-P. Pelteret, B. Turcksin, D. Wells, and S. Zampini, The deal.II library, version 9.5, J. Numer. Math. **31**, 231 (2023).

[52] B. Cockburn, G. E. Karniadakis, and C.-W. Shu, The development of discontinuous Galerkin methods, *Discontinuous Galerkin Methods* (Springer, Berlin, 2000), pp. 3–50.

[53] B. Cockburn, Discontinuous Galerkin methods, Z. Angew. Math. Mech. **83**, 731 (2003).

[54] D. N. Arnold, F. Brezzi, B. Cockburn, and L. D. Marini, Unified analysis of discontinuous Galerkin methods for elliptic problems, SIAM J. Numer. Anal. **39**, 1749 (2002).

[55] F. Brezzi, L. D. Marini, and E. Süli, Discontinuous Galerkin methods for first-order hyperbolic problems, Math. Models Methods Appl. Sci. **14**, 1893 (2004).

[56] R. Grein, T. Löfwander, and M. Eschrig, Inverse proximity effect and influence of disorder on triplet supercurrents in strongly spin-polarized ferromagnets, Phys. Rev. B **88**, 054502 (2013).

[57] C. Johnson, *Numerical Solution of Partial Differential Equations by the Finite Element Method (Dover Books on Mathematics)* (Dover Publications, Mineola, NY, 2009).

[58] T. Ozaki, Continued fraction representation of the Fermi-Dirac function for large-scale electronic structure calculations, Phys. Rev. B **75**, 035123 (2007).